Space–Time Characteristics of Areal Reduction Factors and Rainfall Processes

KORBINIAN BREINL[a]

Institute of Hydraulic Engineering and Water Resources Management, Vienna University of Technology, Vienna, Austria, and Centre of Natural Hazards and Disaster Science, Uppsala, Sweden

HANNES MÜLLER-THOMY[b] AND GÜNTER BLÖSCHL[c]

Institute of Hydraulic Engineering and Water Resources Management, Vienna University of Technology, Vienna, Austria

(Manuscript received 24 September 2019, in final form 12 February 2020)

ABSTRACT

We estimate areal reduction factors (ARFs; the ratio of catchment rainfall and point rainfall) varying in space and time using a fixed-area method for Austria and link them to the dominating rainfall processes in the region. We particularly focus on two subregions in the west and east of the country, where stratiform and convective rainfall processes dominate, respectively. ARFs are estimated using a rainfall dataset of 306 rain gauges with hourly resolution for five durations between 1 h and 1 day. Results indicate that the ARFs decay faster with area in regions of increased convective activity than in regions dominated by stratiform processes. Low ARF values occur where and when lightning activity (as a proxy for convective activity) is high, but some areas with reduced lightning activity exhibit also rather low ARFs as, in summer, convective rainfall can occur in any part of the country. ARFs tend to decrease with increasing return period, possibly because the contribution of convective rainfall is higher. The results of this study are consistent with similar studies in humid climates and provide new insights regarding the relationship of ARFs and dominating rainfall processes.

1. Introduction

Various applications in hydrology require an understanding of the spatial and temporal behavior of extreme rainfall over a catchment as it impacts the runoff behavior and its scaling characteristics (Allen and DeGaetano 2005a). Research on this topic refers to problem number 6 "What are the hydrologic laws at the catchment scale and how do they change with scale?" of the 23 unsolved problems in hydrology (Blöschl et al. 2019). In engineering practice, point rainfall intensity is only applicable to very small catchments, as already pointed out by Marston (1924) in the early twentieth century. For this reason, areal reduction factors (ARFs) are applied to transform point rainfall into average areal rainfall. The ARF is defined as the ratio between the areal rainfall and the point rainfall, usually using the annual maximum rainfall depths over a given time interval of a couple of hours. ARFs are typically used to generate input for rainfall–runoff modeling with areal design rainfall of a certain return period on an event basis (Müller and Haberlandt 2018). ARFs are typically presented as so-called ARF curves that represent the relationship between ARFs and catchment area. The estimates of ARFs are influenced by 1) the rainfall processes, 2) the magnitude of the events as characterized by the return period, 3) any biases in the rainfall data used, and 4) the estimation method.

1) Various authors describe a relationship between the ARF and different rainfall processes. According to Skaugen (1997), ARFs of spatially small-scale rainfall events in southern Norway recorded at daily resolution decay more rapidly with increasing area compared to large-scale rainfall events. By analyzing rain gauge data in Illinois (United States) at high temporal resolution, Huff and Shipp (1969) revealed

Denotes content that is immediately available upon publication as open access.

[a] ORCID: 0000-0003-0489-4526.
[b] ORCID: 0000-0001-5214-8945.
[c] ORCID: 0000-0003-2227-8225.

Corresponding author: Korbinian Breinl, breinl@hydro.tuwien.ac.at

DOI: 10.1175/JHM-D-19-0228.1

that correlation with distance decayed quickly for thunderstorms and rain showers, whereas the decay was lower for steady rain and passing low pressure centers. Similar results were obtained by Wright et al. (2014). Allen and DeGaetano (2005a) found smaller ARFs in summer than in winter, which they attributed to a higher frequency of convective events. Similar findings were reported by Huff and Shipp (1969). Various authors reported a dependency between the ARFs and the geographical location, which is similarly related to the climate and the dominating local rainfall processes (Asquith and Famiglietti 2000; Omolayo 1993; Skaugen 1997; Zehr and Myers 1984). For short durations, ARFs tend to decay faster with area than for long durations (Mineo et al. 2018; NERC 1975; Ramos et al. 2005), usually due to the predominantly convective nature and small spatial extent of short duration events (Sivapalan and Blöschl 1998). Research also suggests a potential difference in ARFs within urbanized areas and in the countryside as convective processes may be amplified in major metropolitan regions (Huff 1995).

2) The findings on the relationship between ARFs and the rainfall return period are mixed: Skaugen (1997), Sivapalan and Blöschl (1998), Asquith and Famiglietti (2000), Allen and DeGaetano (2005a), Mailhot et al. (2012), and Le et al. (2018) reported that the ARF decreases with increasing return periods, usually due to a higher contribution of convective activity. These results are in contrast with studies in Switzerland by Grebner and Roesch (1997), who did not find a relationship between ARFs and the return period for areas greater than 500 km^2. There were variations for smaller areas, though, which the authors explained with the low density of the rain gauge network being unable to capture convective events, and the relatively short length of the observation records. Wright et al. (2014) did not find a significant relationship either.

3) In terms of the rainfall data, the period of the rainfall time series used can influence estimated ARFs due to the temporal variability of rainfall (Asquith and Famiglietti 2000; Svensson and Jones 2010). Also, the combination of different rain gauge networks to reach an acceptable spatial coverage can lead to bias of the ARF values (Asquith and Famiglietti 2000). The station density and the interpolation techniques have however little influence on ARFs according to Allen and DeGaetano (2005a). Allen and DeGaetano (2005a) state that effects of mountains on rainfall can theoretically affect ARFs. Interpolation methods such as Thiessen polygons do not usually account for the fact that rain gauge networks are sparser at higher altitudes. Considering this effect in spatial interpolation techniques did however not significantly impact the ARFs in the study of Allen and DeGaetano (2005a).

4) Various methods have been proposed to estimate ARFs. Svensson and Jones (2010) classify the different methods into (i) general empirical methods, (ii) specific empirical methods, (iii) spatial correlation structure, (iv) crossing properties, (v) scaling relationships, (vi) storm movement, and (vii) radar data. General empirical methods include fixed-area and storm-centered approaches. As for the first, the areal rainfall from a fixed area and for a specific return period is divided by the point rainfall of the same return period. Storm-centered approaches are similar but with the differences that the area changes with each storm, that the point rainfall is estimated from the highest value of the storm, and that point and areal rainfall are estimated from the same storm. The method of the U.S. Weather Bureau (1957, 1958) is similar to the fixed-area method with the difference that the ratio between areal and point rainfall is not based on the same return period but the mean of areal and point annual maximum time series. NERC (1975) suggest a simplification of the U.S. Weather Bureau (1957, 1958) method, which likewise ignores return periods. Bell (1976) proposes ARFs based on the ratio between annual maximum areal rainfall from Thiessen polygon interpolation and annual maximum point rainfall, thereby considering return periods. Methods based on correlations include the one by Rodriguez-Iturbe and Mejía (1974) who related the ARF to a "characteristic correlation distance" between station pairs, thereby assuming Gaussian point rainfall and a specific correlation structure. Sivapalan and Blöschl (1998) built on the method of Rodriguez-Iturbe and Mejía (1974) but additionally considered the transition from the population of events to extreme values, and thus the return period. Bacchi and Ranzi (1996) proposed a stochastic derivation of ARFs based on crossing properties of the rainfall process aggregated in space in time. The method is suitable for small areas and short durations (Svensson and Jones 2010). De Michele et al. (2001) and Veneziano and Langousis (2005) estimated ARFs based on the scale-invariant behavior of rainfall with a possibility to take return periods into account. Bengtsson and Niemczynowicz (1986) proposed a method using the movement of convective storms. Various authors applied different types of methods using radar data (Allen and DeGaetano 2005b; Durrans et al. 2002; Lombardo et al. 2006;

Olivera et al. 2008). More details on various methods can be found in the comprehensive review by Svensson and Jones (2010). The large number of approaches for deriving ARFs and the large number of eclectic case studies make it difficult to critically examine each method and come up with general recommendations about their applicability. It is therefore of interest to connect ARFs with the predominant hydrometeorology of the region of interest. Not only will an understanding of the hydrometeorology help assess the plausibility of the ARFs estimated, but also the ARFs will contribute to a better understanding of the hydrometeorology as they are a fingerprint of the spatial statistical behavior of extreme precipitation. Additionally, they can help in the testing of spatial statistical models of rainfall (e.g., Müller and Haberlandt 2018).

The aim of this paper is to link dominating rainfall processes to ARFs over all of Austria, by analyzing their space–time distribution for different rainfall durations. Our study includes, but is not limited to, the mapping of ARFs in space. To support this goal, we use countrywide lightning data as a proxy for convective activity, and particularly focus on two regions of Austria dominated by stratiform and convective rainfall processes. To the best of our knowledge, (i) countrywide analyses of ARFs have not yet involved a mapping of the ARFs for improved understanding of the link between ARFs and rainfall processes and (ii) not yet examined the potential of using regional lightning data in such space–time investigations. Our main hypothesis is that the different rainfall processes should be reflected in both the differences in the intensity–duration–frequency (IDF) curves and the ARFs in space and time. In other words, we expected the spatial distribution of ARFs to follow similar spatial patterns as the distribution of lightning activity, that is, a fast decay of the ARFs with area in the predominantly convective regions compared to regions dominated by stratiform rainfall. We use an hourly rain gauge dataset to estimate ARFs across the country, using an empirical fixed-area method.

2. Study area and data

Austria is a predominately mountainous country in central Europe with an area of about 84 000 km^2. There are three major ranges of the Alps running from west to east, including the Northern Calcareous Alps, the Central Alps, and Southern Calcareous Alps. The annual mean temperature ranges from above 11°C in the city of Vienna to −9°C at the highest Alpine summits, which exceed 3500 m MSL (Fig. 1a). The complex mountainous environment comprises temperate oceanic climates, humid continental climates, and subarctic and tundra climates (Peel et al. 2007). The total annual precipitation reaches up to 3000 mm in the High Tauern mountain range in the Central Eastern Alps and is below 500 mm in the north of the province of Lower Austria (see Fig. A1 in appendix A).

To estimate the ARFs, we used hourly rainfall time series from 306 rain gauges across Austria covering a simultaneous recording period of 20 years (1995–2014), hereinafter referred to as rain gauge data. Gaps in the recordings were interpolated using kriging with external drift with elevation as an external drift variable (e.g., Haberlandt 2007). The rain gauge data went through comprehensive quality checks before interpolation. The spatial density of the rain gauge dataset turned out to be too low to support more detailed analyses to examine the relationship between rainfall extremes and lighting information (section 4c). We thus used an additional gridded rainfall dataset from the Integrated Nowcasting through Comprehensive Analysis (INCA) system (3354 grid points). INCA was provided for the years 2003–18 by the Central Institute for Meteorology and Geodynamics (ZAMG) with a 1-h temporal resolution and 5-km spatial resolution. As the INCA algorithms have been changed over time causing inhomogeneities in the time series, ZAMG provided a consolidated dataset for this research, where the most recent INCA algorithm was applied to all available years. The original (i.e., unconsolidated) data are available at 1-km spatial resolution; each grid cell in the consolidated dataset represents the mean rainfall of the grid cell area. INCA is a composite product consisting of numerical weather prediction (NWP) output, surface station observations, and radar rainfall and satellite data. It has been specifically developed for the mountainous domain of Austria by considering topographic effects in the analysis methods (Haiden et al. 2011). While the INCA analyses of some parameters such as temperature or humidity do include numerical weather prediction data, INCA analyses of precipitation are solely based on rain gauge and radar data. Furthermore, the averaged 5-km grid cells and the short time series of only 16 years from INCA do not necessarily allow for reliable analyses of ARFs, but they are considered appropriate to better understand the rainfall–lightning relationship.

We analyzed the rain gauge data for Austria with an additional emphasis on two regions with contrasting dominating rainfall processes: one area dominated by stratiform orographic rainfall in the west of Austria (province of Vorarlberg, about 1600 km^2—blue rain gauges and INCA grid in Fig. 1), and one area in the central parts of the province of Styria (about 1800 km^2—magenta rain gauges and INCA grid in Fig. 1),

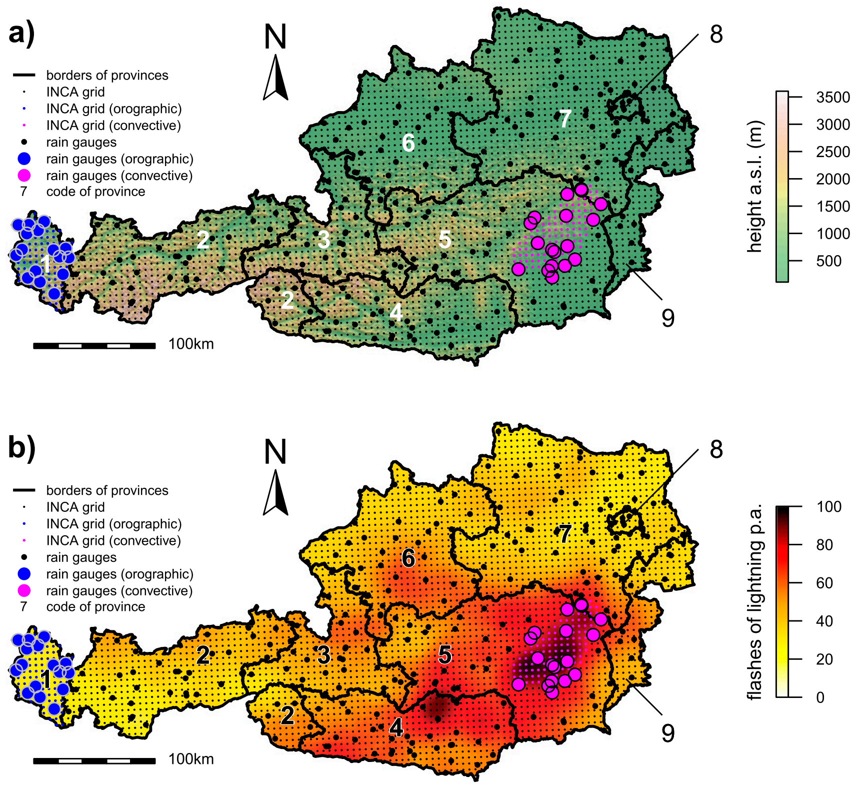

FIG. 1. (a) Distribution of the rain gauges and INCA grid across Austria including the two areas in focus (blue and magenta colors) and the province borders. Numbers refer to the provinces (1 = Vorarlberg, 2 = Tyrol, 3 = Salzburg, 4 = Carinthia, 5 = Styria, 6 = upper Austria, 7 = lower Austria, 8 = Vienna, and 9 = Burgenland. (b) Average annual number of flashes of lightning per square kilometer according to the Austrian Lightning Detection and Information System (ALDIS) for the period 1992–2018 (www.aldis.at) including information on rain gauges and the INCA grid. Rain gauges were used for the ARF analyses, while the INCA grid was used to support additional analyses on the rainfall–lightning relationship.

hereinafter referred to as the ''orographic rainfall region'' and ''convective rainfall region.'' The number of rain gauges is 16 in the orographic rainfall region (105 INCA grid points), and 19 in the convective rainfall region (115 INCA grid points). The orographic rainfall region is characterized by three dominant weather patterns with northwesterly flow causing heavy rainfall (Seibert et al. 2007). These weather patterns [called northwesterly flow, westerly ''Stau'' (the German synonym for orographic lift), and north-northwesterly flow; Seibert et al. 2007] cause high orographic rainfall amounts north of the Alpine divide, which can be depicted from the annual rainfall patterns (Fig. A1). The convective rainfall region is dominated by heavy rainfall from summer thunderstorms. The central-eastern part of the province of Styria as well as the eastern parts of Carinthia are the regions of Austria with the highest frequency of thunderstorms (Fig. 1b). The selection of the rainfall data in the convective rainfall region was conducted using spatial lightning information from the Austrian Lightning Detection and Information System (ALDIS; Schulz et al. 2005). ALDIS includes intracloud lightning as well as cloud-to-ground lightning, which we used as a proxy for convective activity (Fig. 1b). Hence, the two different regions described above with their different dominating rainfall processes were ideal for our analyses.

3. Methodology

In the analysis, we estimated IDF statistics and ARFs in space and time for five rainfall durations (d = 1, 3, 6, 12, 24 h).

a. *Estimation of IDF statistics*

For constructing IDF curves at each location we fitted the generalized extreme value (GEV) distribution to the annual maximum (AMAX) rainfall of duration d using the method of maximum likelihood. The areal IDF curves were estimated similarly by fitting the GEV distribution to areal AMAX rainfall. The cumulative distribution function (CDF) of the GEV distribution is defined as

$$F(x;\mu,\sigma,\zeta)=\exp\left\{-\left[1+\zeta\left(\frac{x-\mu}{\sigma}\right)\right]^{-1/\zeta}\right\},$$

where the parameters μ, σ, and ζ represent the location, the scale, and the shape of the distribution, respectively. Koutsoyiannis (2004a,b) analyzed global rainfall extremes and demonstrated that they are more adequately described by a GEV rather than a Gumbel distribution. Notwithstanding the difficulties with estimating the shape parameter ζ for records smaller than 100 years related to estimation bias and sampling variability, Koutsoyiannis (2004a,b) therefore recommend the use of the GEV distribution over alternative distributions such as the Gumbel distribution. In that context, typical annual maximum rainfall time series with a length between 20 and 50 years hide the GEV distribution and often display Gumbel behavior, although the real behavior of rainfall maxima can be better described by a GEV distribution (Koutsoyiannis 2004b). This is not a peculiarity of the examined records but a generalized statistical effect (Koutsoyiannis and Baloutsos 2000). We also applied model selection using the Akaike information criterion (AIC_c) for short sample sizes (e.g., Burnham and Anderson 2004; Okoli et al. 2018) for the Gumbel and GEV distributions. The AIC_c analysis can be found in appendix B. Based on the analysis of AIC_c and the studies by Koutsoyiannis (2004a,b) and Koutsoyiannis and Baloutsos (2000), we used the GEV distribution for all stations (periods, durations, area sizes). Given the uncertainty of the shape parameter ζ, we did not examine return periods beyond 30 years due to the relatively short length of the time series available (20 years of rain gauge data).

b. *Estimation of ARFs*

Figure 2 provides an overview of the three steps conducted to estimate the ARFs.

1) Variogram modeling (Fig. 2, right): We fitted variogram models for all of Austria, that is, considering all 306 gauge locations g. The procedure was conducted for the five different durations d as well as five periods s, annual (January–December), spring (March–May), summer (June–August), autumn (September–November), and winter (December–February). As the ARFs refer to annual maxima and to ensure that the variogram models better represent extreme rainfall events, we fitted variogram models only taking into account time steps/durations with high areal rainfall amounts. The latter were estimated by computing the arithmetic mean over the entire country for each duration time step from which we only took the upper 10% of for estimating empirical variograms. These empirical variogram models were then averaged over all locations g, and a theoretical variogram model was fitted. We used the exponential model as the theoretical variogram model, which has been proven to be robust across rainfall of different durations in Austria (Skøien and Blöschl 2006), and visual inspection of the resulting variograms confirmed its suitability. The models were fitted without a nugget to avoid steps in the ARF curves for small areas and thus allow for smooth ARF curves across all area sizes. That is, as a result, we obtained 25 variogram models (from five durations for five periods). In a sensitivity study, we conducted the whole study using the rain gauge data fitting variograms to the upper 1% (very extreme events but small sample ratio) and the upper 90% (most types of rainfall events, very high sample ratio) of rainy durations. The final results turned out to be very similar.
2) Block kriging (Fig. 2, top-left area): The estimated variogram models for the rain gauge data served as input for the block kriging methodology (Fig. 2, left area "block kriging"). To the best of our knowledge, block kriging has not yet been applied in the context of ARF research but is an efficient way of achieving this task. To do so we used the statistics package "gstat" version 2.0.2 in the statistical computing software R version 3.6.0 (Pebesma and Wesseling 1998). Block kriging is similar to more commonly applied ordinary kriging (OK) but allows for the estimation of average values over a surface, segment, or volume of any shape and size (e.g., Goovaerts 1997) without interpolating point values over a grid. Gstat assumes the block to have a square shape of a given area, which we assume to approximately represent the shape of catchments. We likewise tested block kriging with external drift (with elevation as drift variable), but differences in the results were negligible. We limited the number of (spatially) nearest observations used for the kriging predictions to 30 for numerical efficiency. Test simulations showed that the results are almost identical with those when using a larger number of observations (see appendix C). Annual maximum point rainfall was estimated at each rain gauge location g, in each period s, for each duration d, and for each year m. Areal annual maximum rainfall for each rain gauge location g, each period s, each duration d, and for each year m was then estimated by block kriging for nine different square block sizes b (1, 3, 5, 10, 30, 50, 100, 300, 500 km^2), using the related variogram models estimated in step 1. The annual maxima for the point and areal rainfall were estimated independently,

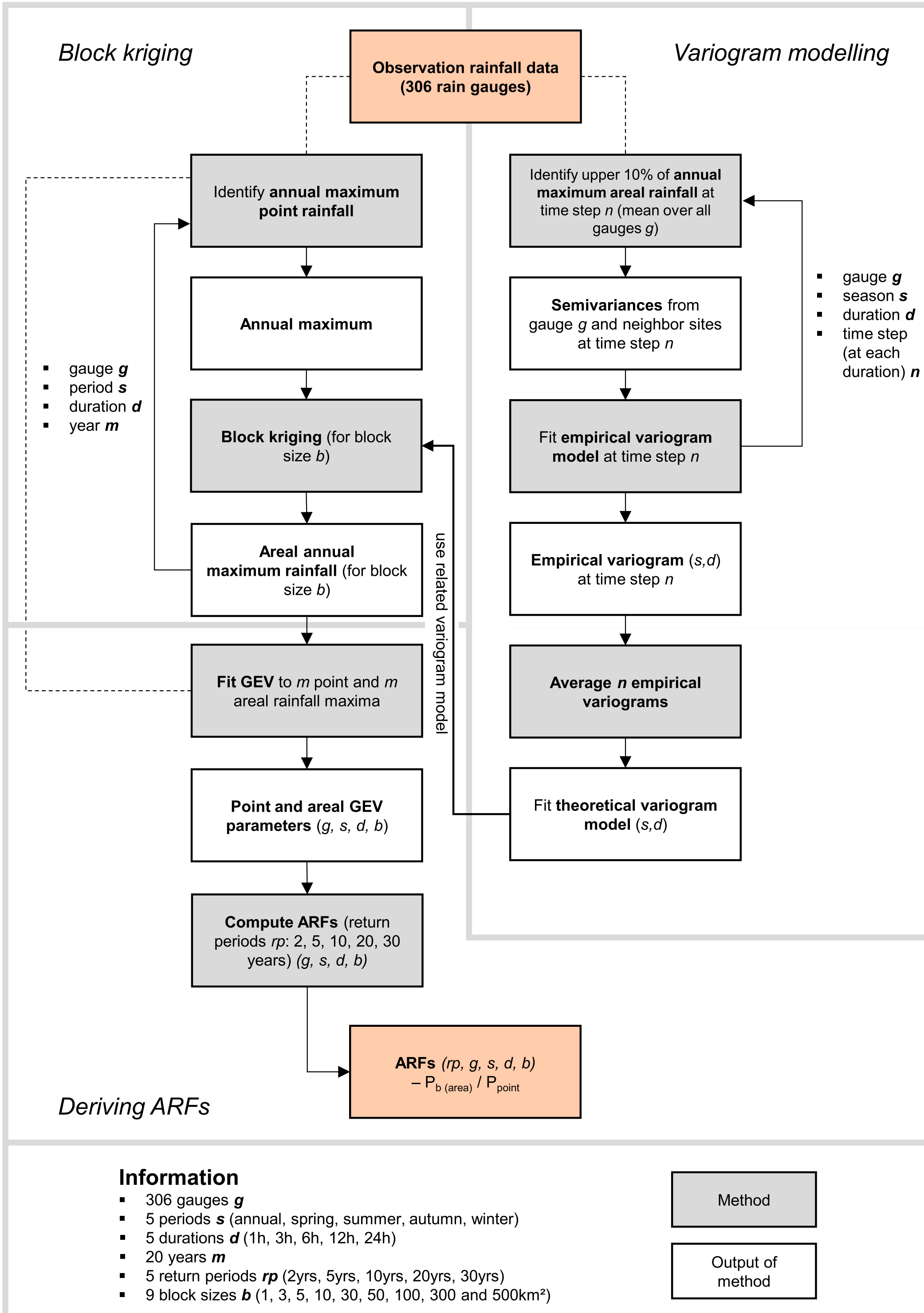

FIG. 2. Schematics of the framework for deriving the areal reduction factors (ARFs), split into (i) the block kriging methodology, (ii) variogram modeling, and (iii) the estimation of the final ARFs.

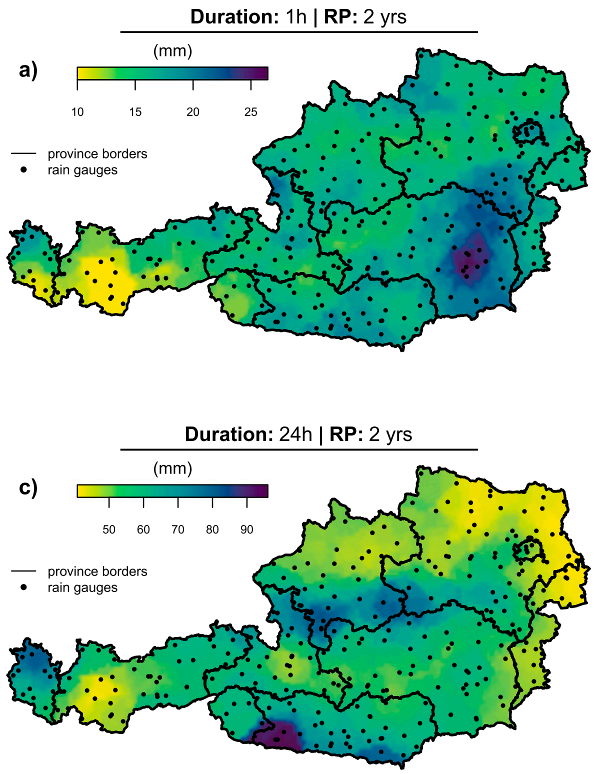

FIG. 3. IDF estimates for different durations (1 and 24 h) and frequencies (2- and 30-yr return periods) across Austria, estimated from the entire time series (i.e., entire year) of the rain gauge data. Maps are based on nearest neighbor interpolation with five nearest neighbors.

that is, the spatial annual maxima do not necessarily coincide with a point annual maximum. As result, we obtained 225 vectors of length $n = 20$ (from 5 periods, 5 durations, and 9 block sizes) for each rain gauge of the rain gauge data.

3) Deriving ARFs (Fig. 2, bottom-left area): To both resulting vectors of the point and areal rainfall maxima we fitted a GEV distribution using the method of maximum likelihood (see section 3a for details on the GEV). Based on the GEV parameters for g, s, d, and b we computed point and areal rainfall for five different return periods (RP; 2, 5, 10, 20, and 30 years). The final ARFs for each return period RP, rain gauge location g, each season s, each duration d, and each area (i.e., block) size b were then computed by the ratio of the areal rainfall P_{areal} and the point rainfall value P_{point}, that is, $P_{\mathrm{areal}}/P_{\mathrm{point}}$.

A limitation behind fitting countrywide variograms to the upper 10% of rainy duration time steps is that strong localized storms may not be represented with this approach as they occur locally, when the rest of the country is relatively dry. By this, the spatial extent of small-scale rainfall events of small durations may be overestimated, which may also overestimate ARFs. We investigated the possibility of fitting variograms separately centered on each single rain gauge to address this issue, varying the number of nearest observations from 10 to 50 gauges. In the majority of cases these local empirical variograms had a very high scatter (especially when using a smaller number of nearest neighbors) and did not give robust fits of the theoretical variogram models. A sensitivity study comparing the local and countrywide variograms at selected rain gauges demonstrated that the global variograms produce lower interpolation biases across all periods and durations and are thus recommended (see appendix C).

As for the block kriging methodology, generally speaking, some kind of interpolation is always needed to estimate the ARFs for different area sizes. As an alternative to our proposed approach, one could interpolate the station values for each time step and each duration over a very fine grid (to be able to estimate small areas), and then average over the areas to estimate the areal rainfall. However, the computational costs become very large. Block kriging does not require the interpolation over a grid but gives identical results. The so-called kriging weights for the rain gauges and each (block-) area size under consideration can be estimated from the variogram models in a much more efficient way.

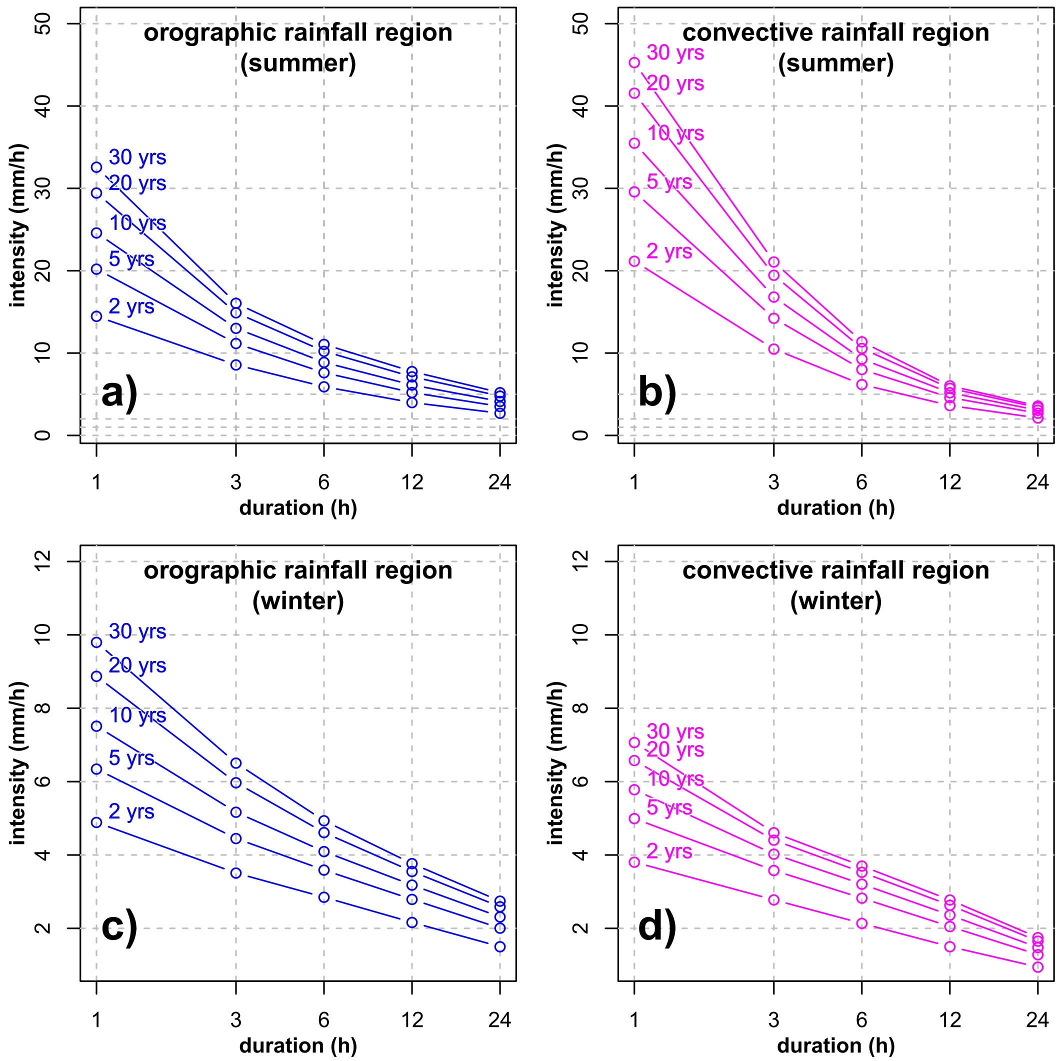

FIG. 4. IDF curves for the (left) orographic and (right) convective rainfall region (right) (see Fig. 1 for regions) in (a),(b) summer and (c),(d) winter. IDF curves are the averages of all rain gauges of the rain gauge data.

To provide further validation of our methodology, we compared interpolation results at six exemplary sites using kriging with local and countrywide variograms as well as (alternative) inverse distance weighting (IDW) interpolation. The results from this sensitivity study justify the block kriging approach with (i) countrywide variograms and (ii) 30 nearest observations (corresponds to a mean maximum distance of 59.5 km over all sites) for the kriging predictions (see appendix C).

4. Results and discussion

a. IDF statistics

IDF rainfall for different durations and frequencies from the rain gauge data are presented in space and time for the entire year (Fig. 3). For 1-h duration and a return period of 2 years (Fig. 3a), the highest rainfall occurs in eastern Styria (see Fig. 1 for the Austrian provinces). The pattern is similar with a higher return period of 30 years (Fig. 3b), differences can be seen for example along the northern border with relatively higher rainfall amounts. For a rainfall duration of 24 h the pattern across Austria is again very similar for low and high return periods (2 and 10 years, Figs. 3c and 3d, respectively), but it differs significantly from the pattern identified for rainfall with 1-h duration (Figs. 3a,b). Regions of high rainfall include the province of Vorarlberg in the west (orographic rainfall region), in the south of Carinthia along the southern Austrian border, and along the north of the Alpine divide in the central parts of Austria.

The high rainfall intensities in eastern Austria (Figs. 3a,b) are in line with high lightning activity (Fig. 1b), which

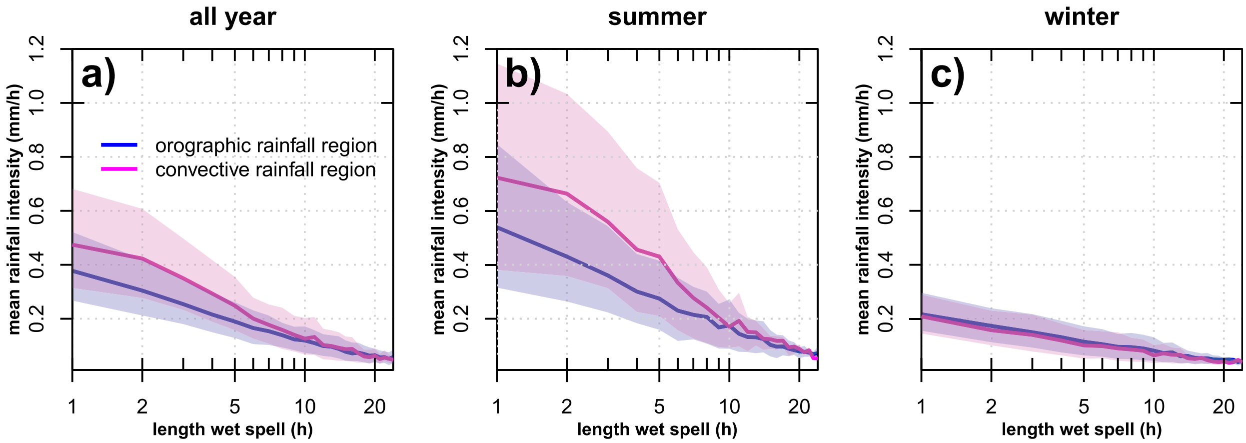

FIG. 5. Intensity of all wet spells recorded in the time series, for the (a) entire year, (b) summer, and (c) winter. Solid lines represent the mean of all wet spells of all gauges in the region. Shaded areas denote the 10th and 90th percentiles of temporal and spatial variability.

suggests convective rainfall as their likely cause. Flash floods are frequent in eastern Austria, especially in southeastern Austria and in northeastern Austria (Merz and Blöschl 2003). The hilly terrain enhances vertical motion in the boundary layer and increases the likelihood of convective storms (Merz and Blöschl 2003). Additionally, the southerly location and thus closeness to the Adriatic Sea, that is, very warm summer temperatures and high atmospheric humidity, may contribute to the high intensities. The spatial distribution of the 24-h rainfall can be related to the dominant circulation patterns, that is, mainly synoptic systems and stratiform rainfall. The regions in Vorarlberg and in central Austria are characterized by heavy rainfall from three different dominant synoptic patterns called northwesterly flow, westerly "Stau" (the German synonym for orographic lift), and north-northwesterly flow (Hofstätter et al. 2018; Seibert et al. 2007), that is, stratiform orographic rainfall from air masses from predominantly northwest directions. The most frequent pattern is the northwesterly flow, where low level trajectories come from the Atlantic Ocean, thus transporting humid air. The westerly Stau and the north-northwesterly flow are characterized by higher wind speeds compared to the northwesterly flow. The high rainfall across the southern border in Carinthia is to a large degree related to the southerly Stau pattern, that is, southerly flow at higher and lower levels (Seibert et al. 2007). Airflow at low levels supports advection of humidity from the Mediterranean Sea, which is precipitated over the Alps (Seibert et al. 2007). As the four synoptic patterns mentioned above are the most frequent ones across Austria causing most of the rainfall, the pattern of the 24-h IDF estimates (Figs. 3c,d) show clear similarities with the pattern of annual rainfall in Austria (Fig. A1).

Figure 4 presents the IDF curves in the two regions with dominant convective and orographic rainfall, stratified by season and averaged over all rain gauges of the related region. In summer, rainfall intensities are lower in the orographic rainfall region across all return periods (Fig. 4a) for short durations (1, 3 h) compared to the convective rainfall region (Fig. 4b). While intensities are similar for a duration of 6 h, intensities become higher in the orographic rainfall region with long durations (12, 24 h) compared to the convective rainfall region. The IDF curves for summer thus show the dominant convective activity in the convective rainfall region in summer, while orographic processes and long-duration storms are less relevant than in the orographic rainfall region. The precipitation is generally lower in winter, and in particular in the convective rainfall region compared to the orographic rainfall region (Figs. 4c,d). In winter, there is almost no lightning activity. According to the monthly ALDIS statistics, only 0.14% of all flashes recorded in the period 1992–2018 were recorded in winter, while 81.4% were recorded in summer (www.aldis.at).

We also examined how the IDF statistics relate to the characteristics of wet spell intensities in the different regions. Figure 5 summarizes the results. We present results for the intensities of wet spell lengths up to 24 h on an annual basis (Fig. 5a), for the summer period (Fig. 5b) and for winter (Fig. 5c). In general, intensities decrease with longer durations, a phenomenon that has been observed in other studies (Haddad and Rahman 2014; Poduje and Haberlandt 2018). On an annual basis (Fig. 5a), the intensity of wet spells is on average higher in the convective rainfall region compared to the orographic rainfall region, for short durations. This is related to more intense downpours from convective activity.

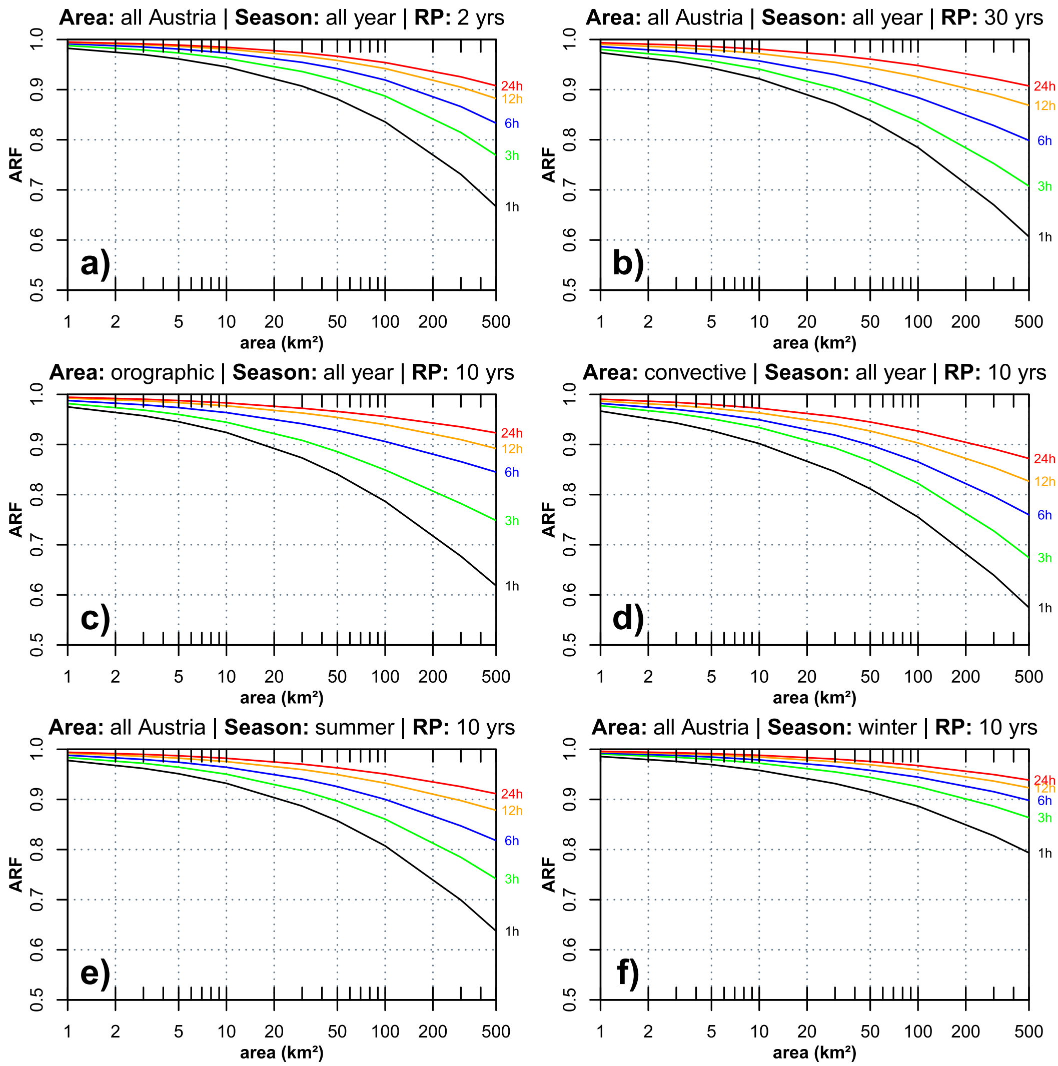

FIG. 6. Areal reduction factors (ARFs) for different return periods, seasons, for all of Austria and the two study regions based on the rain gauge data. Comparisons are shown for (a),(b) two return periods, (c),(d) two regions, and (e),(f) summer and winter.

On average, intensities are 25.2% higher in the convective rainfall region for durations up to 5 h, and 12.1% between 6 and 10 h. Beyond 10 h duration, intensities become very similar. The effect is even more pronounced in the summer period for shorter spell lengths (Fig. 5b), where intensities are generally higher in both study areas. On average, in the convective rainfall region, intensities are 33.3% higher for lengths up to 5 h and 16.5% for length between 6 and 10 h. Intensities are similar for the winter period (Fig. 5c), but on average, intensities are 10.7% lower in the convective rainfall region compared to the orographic rainfall region for wet spell lengths up to 24 h. This is most likely related to the lack of convective storms in this season. In summary, the characteristics of wet spells to a large degree confirm the rainfall processes in the two regions in focus as discussed above.

b. *Areal reduction factors in space and time*

Figure 6 shows some of the ARF results. It is clear that the ARFs change with the return period of the rainfall. For example, for a duration of 1 h, the ARF for a 2-yr rainfall and 100 km^2 is 0.84 while the corresponding estimate for a 30-yr return period is 0.78. Several authors have detected decreasing ARFs with increasing return periods (e.g., Allen and DeGaetano 2005a; Asquith and Famiglietti 2000; Le et al. 2018; Mailhot et al. 2012), although they do not provide precise numbers and focus on considerably larger areas. The differences are assumed to be related to the areal rainfall becoming

TABLE 1. ARFs from fixed-area methods for different area sizes and durations from the present study in comparison with results from other regions. Numbers refer to different (or no) return periods (RPs) in years (yr).

Area (km^2)/ duration (h)	Austria (present study)—RP = 2 yr	South Korea (Kang et al. 2019)—RP = 20 yr	Germany (Verworn 2008)—RP = 10 yr	Australia without dry inland area (Myers and Zehr 1980)—RP = 2 yr	United Kingdom (NERC 1975)—no RP	United States (Ohio Valley, Southeastern U.S., Middle Atlantic region, Northeastern U.S., Great Lakes region) (U.S. Weather Bureau 1957)—no RP
100/1	0.84	0.85	0.74	0.80	0.85	0.85
500/1	0.67	0.71	0.61	0.72	0.72	0.72
100/6	0.92	0.96	0.95	0.92	0.94	0.94
500/6	0.83	0.90	0.88	0.88	0.87	0.87

relatively smaller due to increasing convective activity. ARFs differ between the orographic and convective rainfall regions (Figs. 6c and 6d, curves from different study areas averaged). For example, for a duration of 1 h, the ARF in the orographic rainfall region for a 2-yr rainfall and 100 km^2 is 0.78 while the corresponding estimate in the convective rainfall region for a 30-yr return period is 0.75. The smaller ARFs in the convective study area (Fig. 6d) would be expected due to the dominance of strong convective events. As convective events tend to be smaller than stratiform rainfall events, stronger decays of the ARFs with increasing catchment area will result. The results from other return periods (e.g., 30 years, not shown here) are very similar in respect due to the relative differences between the orographic rainfall region and the convective rainfall region. ARFs are smaller in summer than in the winter (Figs. 6e,f). This would be expected due to the dominance of convective rainfall processes in summer and the dominance of synoptic precipitation processes in winter in Austria.

Overall, the ARF estimates are similar to fixed-area related results from other humid climates across the globe (see Table 1).

Figure 7 shows maps of the ARFs for two rainfall durations (1 and 24 h) and two area (block) sizes (50 and 500 km^2), for a return period of 10 years. The maps were generated by nearest neighbor interpolation with five nearest neighbors for visualization purposes. As can be seen, the ARFs show little spatial variability for 1-h duration and an area of 50 km^2 (Fig. 7a). For example, for the duration of 1 h, which is relevant for convective events, there is no noticeable difference between the orographic rainfall region and convective rainfall region for 50 km^2 (Fig. 7a). The pattern becomes patchier for a catchment of 500 km^2 (Fig. 7b). The general pattern shows similarities with the distribution of the lightning frequency as an indicator of convective activity with smaller ARFs in regions of higher lightning frequency, also see Fig. 1b), such as Carinthia and Styria. However, there are also low values in the western parts of Austria with less lightning activity, which we discuss in more detail in section 4c.

The spatial distribution of the ARFs is similar for 24 h (Figs. 7c,d) and 50 km^2 with little spatial variability (Fig. 7c). For a catchment area of 500 km^2 the region of Styria gives particularly low ARFs, which is likely related to the dominance of convective rainfall (Fig. 7d). However, the relative spatial differences in ARFs are lower for 24 h than for 1 h. For example, the ARFs decrease on average by 21.1% when increasing the area from 50 to 500 km^2 for a 1-h duration (Figs. 7a,b) (average computed over the entire interpolated grid), while

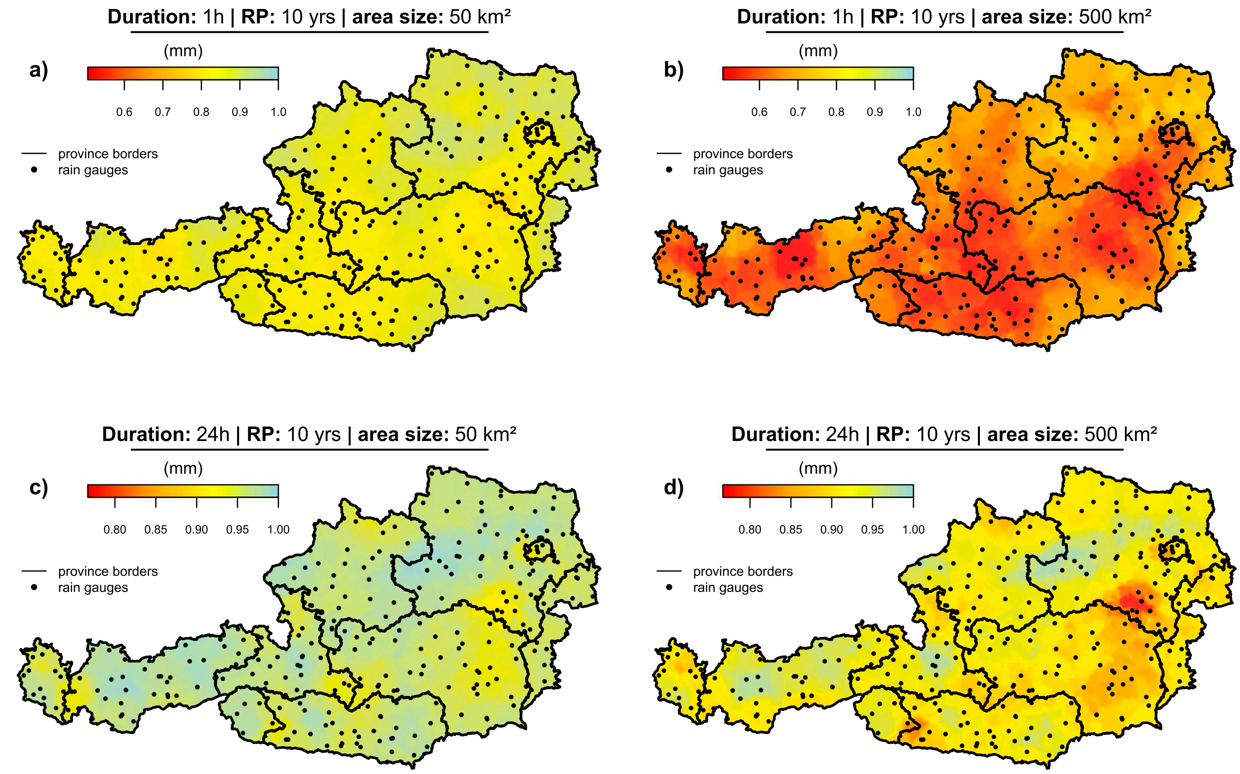

FIG. 7. ARFs for a return period of 10 years, two durations (1 and 24 h) and two catchment sizes (50 and 500 km^2), estimated from the rain gauge dataset.

they only decrease by 6.0% for a 24-h duration (Figs. 7c,d). The differences suggest that, at 1-h duration, convective events dominate, while at 24-h duration synoptic weather systems and stratiform rainfall are more important.

c. ARFs in context of lightning data

To better understand the situation in the west of Austria with its smaller-than-expected ARFs for 1 h in both analyses, the lightning data were analyzed in more detail. While we received the aggregated lightning data with the average number of flashes of lightning for the period 1992–2018 at a 5-km grid from ALDIS (Fig. 1b) to support the identification of the main rainfall processes across the country, we also received a detailed dataset for the year 2012 (5-km grid, lightning information for every ALDIS grid cell and day). We linked the (spatially more dense) annual maxima of INCA rainfall to lightning information, to examine their relationship. To do so, we assigned the maximum number of flashes from ALDIS on the date of the maximum rainfall to each INCA grid cell (INCA to have a very high spatial coverage), using a 10-km radius. Lightning can strike at some distance from the core of a convective cell and 10 km is a typical rule of thumb used by weather forecasters (Walsh et al. 2013). That is, for the year 2012 we got one data point for each grid cell.

Figure 8 provides an overview of the association of INCA annual maximum rainfall with lighting for Austria (Fig. 8a), the orographic rainfall region (Fig. 8b) and the convective rainfall region (Fig. 8c). Specifically, the figure shows the percentage of annual rainfall maxima associated with lightning (i.e., at least one flash within 10 km from the rain gauge). As can be seen, the lightning activity decreases with increasing duration, indicating a change in rainfall processes. Overall, the lightning activity is higher in the convective rainfall region compared to the orographic rainfall region. The slight increase in winter (Figs. 8a,b) for long durations and the absence of lightning in the convective rainfall region may be an artifact of the small sample size, as only one year of daily lightning data could be obtained.

The detailed lightning data provide an explanation of the relatively small ARFs in the west of Austria despite the general dominance of stratiform orographic rainfall in the region. One explanation is that strong Stau events may lead to sharp small-scale contrasts in rainfall totals, such as is typically the case in the orographic rainfall region. However, convective activity provides another explanation: in the orographic rainfall region, 84.8% of

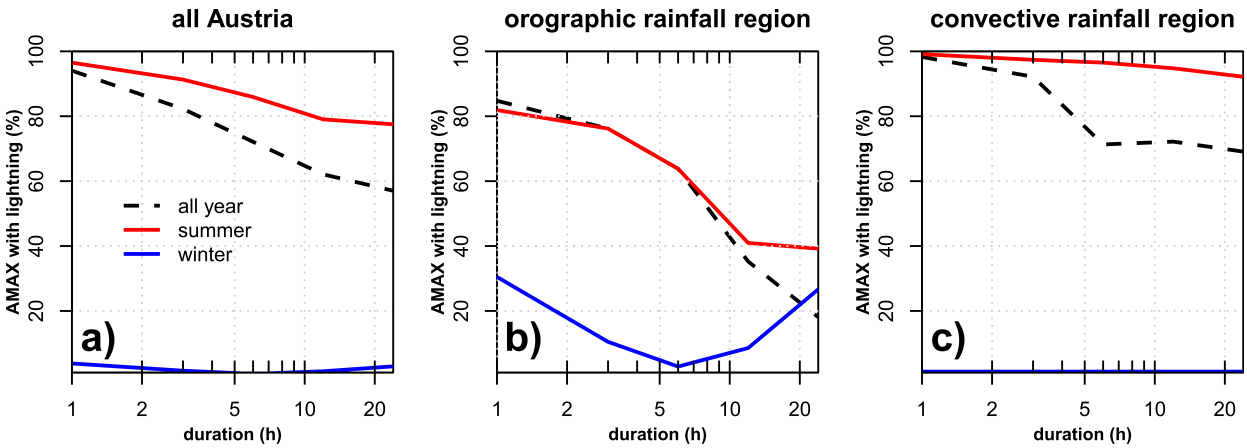

FIG. 8. Percentage of AMAX with different durations associated with lightning for (a) Austria, (b) the orographic rainfall region, and (c) the convective rainfall region, for the entire year, summer, and winter. The lightning statistics are estimated from the ALDIS dataset for the year 2012.

the hourly annual maxima were associated with lightning activity in 2012 (Fig. 8b), in the convective rainfall region these were 98.3% (Fig. 8c). The corresponding average number of flashes per annual maximum was 31.7 and 5.1. That is, it is valid to assume that convective activity is associated with summer extremes in both areas.

To gain further insights into the role of convective activity, we investigated the synchronicity of the dates of the annual rainfall maxima in both regions across all grid points. A large number of annual maxima occurring simultaneously would point toward stratiform events, as events covered a larger area. It turned out that annual maxima in the orographic rainfall region can be related to eleven different dates (and thus most likely different events), while annual maxima in the convective rainfall region can be related to seven different dates. The areas covered by the events on each date were also similar. On average, the annual maxima in the orographic rainfall region were related to a maximum distance between grid points of 26.4 km, while in the convective rainfall region the average maximum distance was 27.1 km. The small sample size from only one year of detailed lightning data does not allow us to draw final conclusions but does provide a plausible indication of convective activity in both regions on the dates of annual maxima. This would explain the similarity of the ARFs in the two regions despite different (generally) dominating rainfall processes.

d. *Limitations*

One limitation in this study is the variograms used. As described above (section 3b), to reach stable fits of the theoretical variogram models, we estimated the empirical variograms for the upper 10% of rainy duration time steps based on the countrywide (and thus based on a large sample size) mean rainfall. Using the same variogram throughout the country may lead to underestimating the spatial variability of the ARFs, but fitting local variograms to address this limitation tended to result in higher interpolation biases, very likely resulting from less robust fits of the theoretical variogram models. In general, longer rainfall time series would probably allow more robust fits of the extreme value distributions (section 3a). Finally, additional detailed lightning data would help better understand the detailed rainfall processes behind annual rainfall extremes (section 4c).

5. Conclusions

The findings of the paper allow us to draw the following conclusions:

- We proposed a new method of estimating ARFs based on block kriging, which is computationally more efficient than interpolating each duration time step and each area size of the entire time series across the domain at high resolution to estimate the ARFs.
- ARFs tend to decay faster in areas with dominant convective activity than in areas with dominating stratiform rainfall, visible in both classic (regional) IDF curves and in space (maps). This finding is consistent with the original hypothesis of the paper as well as with findings from numerous authors (e.g., Allen and DeGaetano 2005a; Huff and Shipp 1969; Skaugen 1997; Wright et al. 2014).
- Lightning information can be a useful proxy for convective activity and thus the magnitude of areal reduction factors in space and time, which was likewise related to our main hypothesis. However, the usefulness

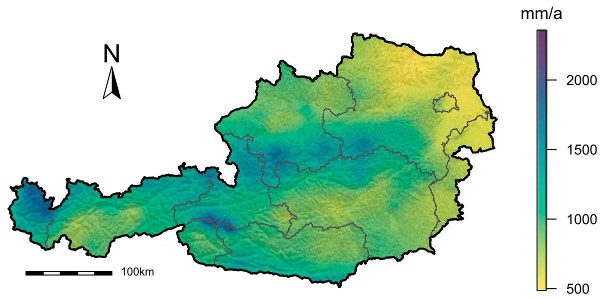

FIG. A1. Annual average rainfall in Austria derived from the rain gauge data. The map is based on nearest neighbor interpolation with five nearest neighbors.

of lightning data in ARF analyses is also limited, at least in the case of Austria, as relatively low ARFs can also occur in areas with relatively low lightning activity, for example in the orographic rainfall region in the west. As the detailed analysis of lightning data for one year revealed, there is a general tendency across Austria that annual maxima are associated with convective activity, leading to reduced ARF values.

- The (countrywide) magnitudes of the ARFs estimated in Austria are similar to those from other studies conducted in humid climates using fixed area methods (e.g., Kang et al. 2019; Myers and Zehr 1980; NERC 1975; U.S. Weather Bureau 1957, 1958; Verworn 2008). For example, for 1-h duration and an area of 100 km^2 (RP = 2 years), we estimated an ARF of 0.84 while the mean of five other studies was 0.82. For 6-h duration and 500 km^2 (RP = 2 years), we estimated an ARF of 0.83 (mean of other studies 0.88).

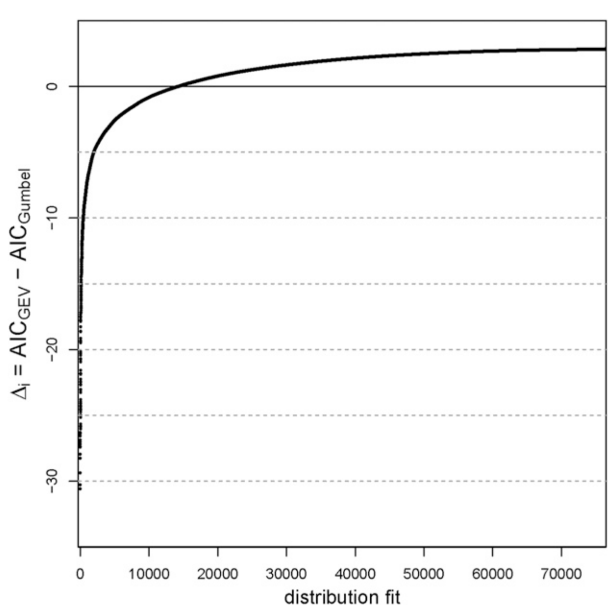

FIG. B1. Analysis of AIC$_c$. Plot shows $\Delta_i = AIC_{GEV} - AIC_{Gumbel}$ of all distribution fits (all periods, all durations, all area sizes, all years) sorted by value. Values below 0 indicate selection of the GEV, and values above 0 indicate selection of the Gumbel.

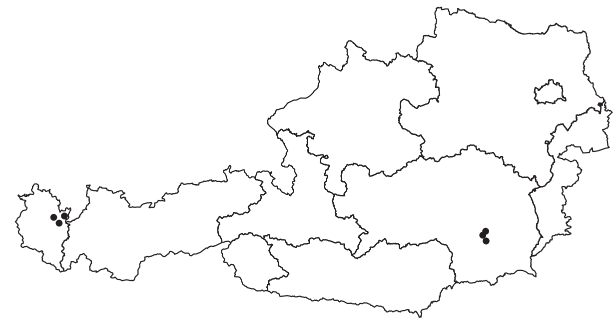

FIG. C1. Six rain gauges (three in the west, three in the east) selected for additional tests to validate the kriging interpolation method.

- The areal reduction factors decrease with the return period, which matches findings of other authors (e.g., Allen and DeGaetano 2005a; Asquith and Famiglietti 2000; Le et al. 2018; Mailhot et al. 2012; Sivapalan and Blöschl 1998). This decrease is most pronounced for durations shorter than 24 h. This decrease may possibly be observed because the contribution of convective rainfall is higher.
- For future research, it would be interesting to investigate how the process links of the ARFs analyzed here relate to the space–time scaling of floods, which is the main natural hazard in terms of monetary losses in Austria.

Acknowledgments. This research has received funding from the European Union's Horizon 2020 research and innovation programme under the Marie Sklodowska-Curie Grant Agreement STARFLOOD 793558 (www.starflood.at). Hannes Müller-Thomy acknowledges the funding from the Research Fellowship (MU 4257/1-1) by DFG e.V., Bonn, Germany. This research has received funding from the Austrian Federal Ministry for Sustainability and Tourism and the Bavarian Environment Agency in the framework of the project WETRAX+. We thank the Central Institution for Meteorology and Geodynamics for providing the rain gauge and INCA data. We thank Wolfgang Schulz and ALDIS for providing the lightning data. Helpful discussions with Thea Turkington, David Lun, and Jürgen Komma on our work as well as detailed comments from two anonymous reviewers and the editor are gratefully acknowledged.
Data availability statement: The rain gauge data used in this study can be obtained from the Central Institution for Meteorology and Geodynamics (ZAMG)

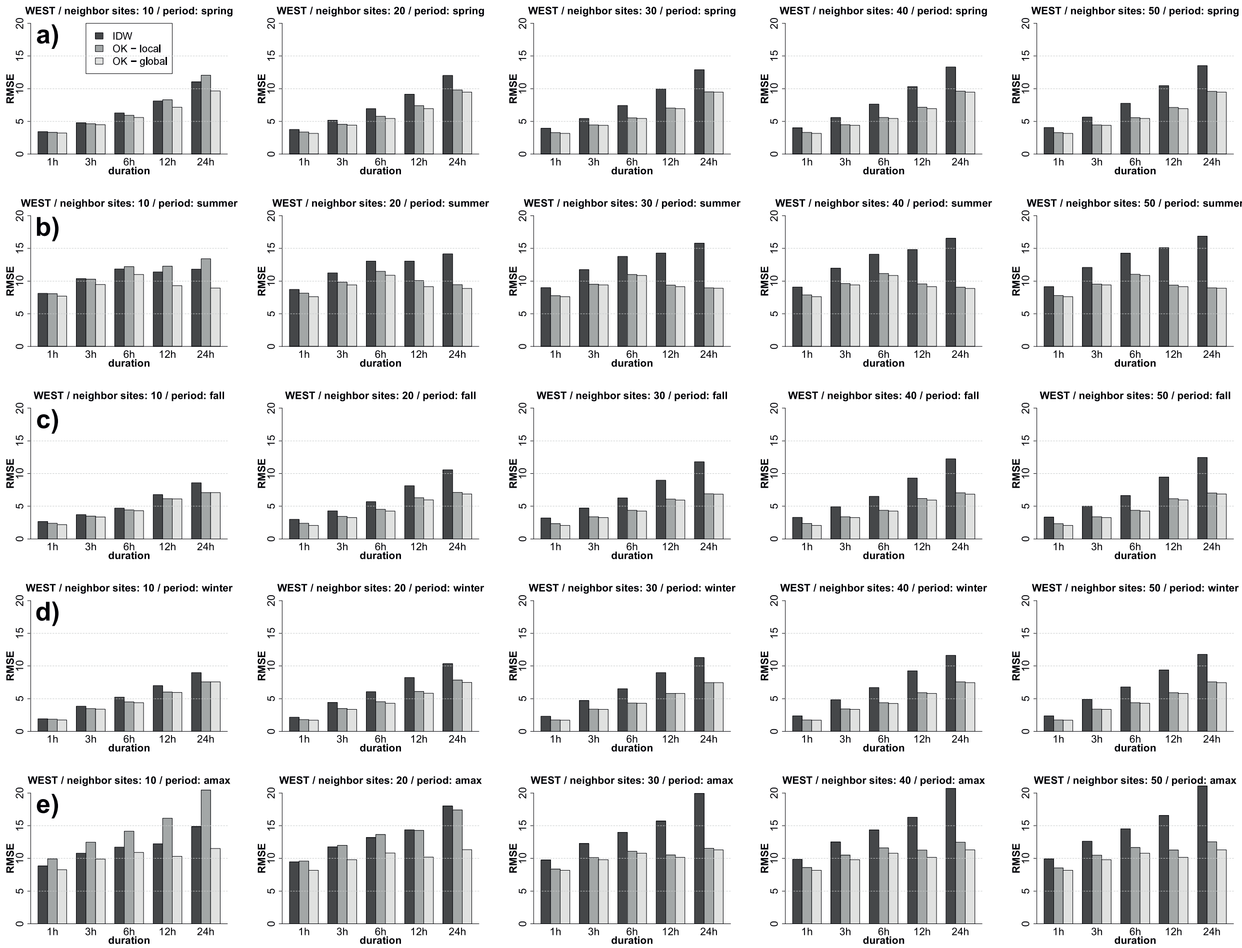

FIG. C2. RMSE from three different interpolation methods averaged over the three gauges and all years in the west of Austria, namely, IDW and OK with local and global (i.e., countrywide) variograms. Results are presented across the different periods (a) spring, (b) summer, (c) fall, (d) winter, and (e) annual maxima from the entire year (AMAX). The number of neighbor sites is varied from 10 to 50 neighbors.

(www.zamg.ac.at). The lightning data used can be obtained from the Austrian Lightning Detection and Information System (ALDIS) (www.aldis.at).

APPENDIX A

Additional Figure

Figure A1 shows the annual average rainfall in Austria derived from the rain gauge data.

APPENDIX B

AIC$_c$ Analysis

The Gumbel distribution produced the lowest AIC$_c$ in the majority of the rain gauges (77%). However, according to Burnham and Anderson (2004), one must also consider the AIC differences, that is, $\Delta_i = \mathrm{AIC}_i - \mathrm{AIC}_{\min}$ over all candidate models examined. Models with $\Delta_i \leq 2$ have substantial support, models with $4 \leq \Delta_i \leq 7$ have considerably less support, models with $\Delta_i > 10$ have essentially no support (Burnham and Anderson 2004). For our time series, we plotted $\Delta_i = \mathrm{AIC}_{\mathrm{GEV}} - \mathrm{AIC}_{\mathrm{Gumbel}}$, that is, a positive value means selection of Gumbel and a negative value means selection of GEV. As can be seen in Fig. B1, when AIC$_c$ suggests Gumbel, both the Gumbel and GEV are essentially valid according to Burnham and Anderson (2004) with Δ_i not exceeding a value of 2.9. The opposite does not apply, that is, the GEV is considerably more supported when suggested by AIC$_c$ as Δ_i can get negative values of a much larger magnitude. Based on the analysis of AIC$_c$ and the studies by Koutsoyiannis (2004a,b); Koutsoyiannis and Baloutsos (2000), we used the GEV distribution for all stations (periods, durations, area sizes) (i) for the sake of consistency and (ii) to address the issue of the Gumbel not being supported for a larger number of fits.

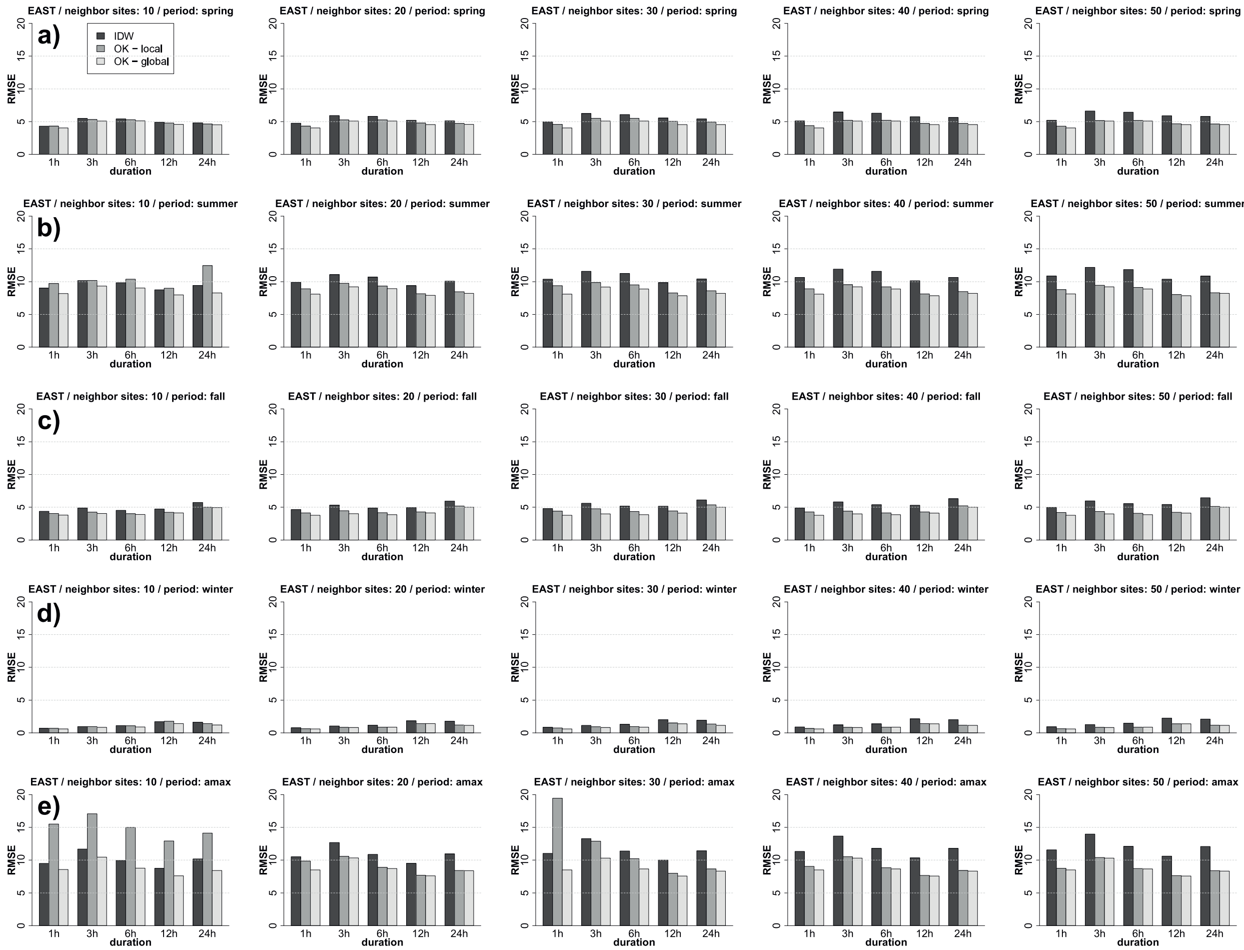

FIG. C3. RMSE from three different interpolation methods averaged over the three gauges and all years in the east of Austria, namely, IDW and OK with local and global (i.e., countrywide) variograms. Results are presented across the different periods (a) spring, (b) summer, (c) fall, (d) winter, and (e) annual maxima from the entire year (AMAX). The number of neighbor sites is varied from 10 to 50 neighbors.

APPENDIX C

Validation of the Kriging Interpolation Method

We selected six rain gauges (three in the west and three in the east of Austria, Fig. C1), to further validate the kriging interpolation method.

We conducted interpolations with the point rainfall across the different five periods (annual maxima and four seasons), thereby using inverse distance weighting (IDW), ordinary kriging (OK) with local variograms fitted to the 10, 20, 30, 40, and 50 nearest neighbors (corresponds to a mean maximum site distance over all sites of 30.6, 46.3, 59.5, 72.0, and 84.1 km), and OK with

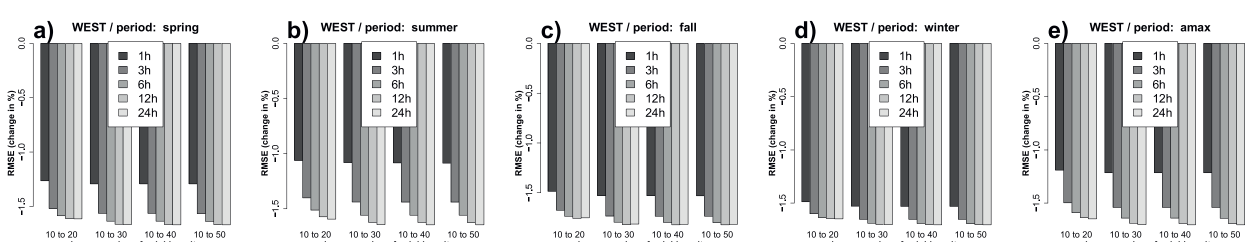

FIG. C4. Change in the RMSE averaged over the three gauges and all years in the west, when varying the number of neighbors with OK and global variograms from 10 to 50 neighbor sites. Results are presented across the different periods (a) spring, (b) summer, (c) fall, (d) winter, and (e) annual maxima from the entire year (AMAX) and across different durations. Results are presented as changes in the RMSE when using 20 instead of 10 nearest neighbors (10 to 20), 30 instead of 10 sites (10 to 30), and so forth.

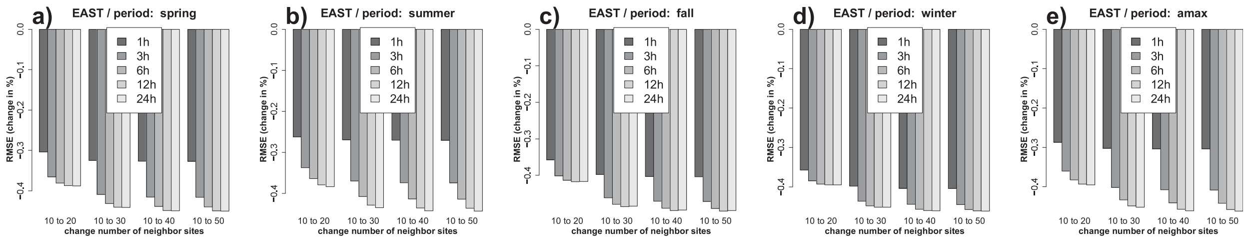

FIG. C5. Change in the RMSE averaged over the three gauges and all years in the east, when varying the number of neighbors with OK and global variograms from 10 to 50 neighbor sites. Results are presented across the different periods (a) spring, (b) summer, (c) fall, (d) winter, and (e) annual maxima from the entire year (AMAX) and across different durations. Results are presented as changes in the RMSE when using 20 instead of 10 nearest neighbors (10 to 20), 30 instead of 10 sites (10 to 30), and so forth.

global (i.e., countrywide) variograms. The actual rainfall value at the location of the rain gauge was left out (leave-one-out analysis). The rainfall value at the location was estimated with one of the methods and setups. In the case of OK with local variograms, the OK itself was conducted using the same number of nearest neighbors as used for estimating the variograms, that is, when a local variogram fitted to 10 nearest neighbors was used, the same number of 10 nearest neighbors was used in the OK procedure itself and so on. In case of the global variograms, the number of sites considered in the OK procedure itself was likewise varied between 10 and 50.

Figure C2 summarizes the results for the three rain gauges in the west of Austria. As can be seen, across all periods and durations (Figs. C2a–e), OK with the global variograms produces the lowest RMSE. While the number of neighbors considered for OK with local variograms has noticeable influence (decreasing bias with increasing number of neighbors), the number of neighbors considered when conducting OK with global variograms hardly influences the results. In general, the results are comparable in the east of Austria (Fig. C3) with OK producing the lowest bias when using global variograms.

Our study confirms other studies on rainfall interpolation, which state that kriging is preferred compared to other more simplistic methods such as IDW or nearest neighbor interpolation (e.g., Haberlandt 2007; Mair and Fares 2011; Wagner et al. 2012).

While the tests revealed that OK with global variograms is the interpolation method producing the lowest bias, we take a closer look into the number of gauges considered in the OK itself. This information is contained in Figs. C2 and C3 but hardly visible. Figure C4 shows the bias for the three gauges in the west from OK with global variograms with varying number of neighbors, in relation to the minimum number of 10 nearest neighbors across the five periods and across durations. As can be seen, the reduction of the bias reaches a minimum when considering 30 nearest neighbors but does not noticeably further decrease with 40 or 50 sites.

The results are similar for the three gauges in the east (Fig. C5). In all periods and with all durations, 30 neighbor sites appear to be a reasonable number.

REFERENCES

Allen, R. J., and A. T. DeGaetano, 2005a: Areal reduction factors for two eastern United States regions with high rain-gauge density. *J. Hydrol. Eng.*, **10**, 327–335, https://doi.org/10.1061/(ASCE)1084-0699(2005)10:4(327).

——, and ——, 2005b: Considerations for the use of radar-derived precipitation estimates in determining return intervals for extreme areal precipitation amounts. *J. Hydrol.*, **315**, 203–219, https://doi.org/10.1016/j.jhydrol.2005.03.028.

Asquith, W. H., and J. S. Famiglietti, 2000: Precipitation areal-reduction factor estimation using an annual-maxima centered approach. *J. Hydrol.*, **230**, 55–69, https://doi.org/10.1016/S0022-1694(00)00170-0.

Bacchi, B., and R. Ranzi, 1996: On the derivation of the areal reduction factor of storms. *Atmos. Res.*, **42**, 123–135, https://doi.org/10.1016/0169-8095(95)00058-5.

Bell, F. C., 1976: The areal reduction factor in rainfall frequency estimation. Institute of Hydrology, Rep. 35, Natural Environment Research Council, Swindon, United Kingdom, 85 pp.

Bengtsson, L., and J. Niemczynowicz, 1986: Areal reduction factors from rain movement. *Nord. Hydrol.*, **17**, 65–82, https://doi.org/10.2166/nh.1986.0005.

Blöschl, G., and Coauthors, 2019: Twenty-three UNSOLVED PROBLEMS IN HYDROlogy (UPH) – A community perspective. *Hydrol. Sci. J.*, **64**, 1141–1158, https://doi.org/10.1080/02626667.2019.1620507.

Burnham, K. P., and D. R. Anderson, 2004: Multimodel inference: Understanding AIC and BIC in model selection. *Sociol. Methods Res.*, **33**, 261–304, https://doi.org/10.1177/0049124104268644.

De Michele, C., N. T. Kottegoda, and R. Rosso, 2001: The derivation of areal reduction factor of storm rainfall from its scaling properties. *Water Resour. Res.*, **37**, 3247–3252, https://doi.org/10.1029/2001WR000346.

Durrans, S. R., L. T. Julian, and M. Yekta, 2002: Estimation of depth-area relationships using radar-rainfall data. *J. Hydrol. Eng.*, **7**, 356–367, https://doi.org/10.1061/(ASCE)1084-0699(2002)7:5(356).

Goovaerts, P., 1997: *Geostatistics for Natural Resources Evaluation*. Oxford University Press, 483 pp.

Grebner, D., and T. Roesch, 1997: Regional dependence and application of DAD relationships. *IAHS Publ.*, **246**, 223–230.

Haberlandt, U., 2007: Geostatistical interpolation of hourly precipitation from rain gauges and radar for a large-scale extreme rainfall event. *J. Hydrol.*, **332**, 144–157, https://doi.org/10.1016/j.jhydrol.2006.06.028.

Haddad, K., and A. Rahman, 2014: Derivation of short-duration design rainfalls using daily rainfall statistics. *Nat. Hazards*, **74**, 1391–1401, https://doi.org/10.1007/s11069-014-1248-7.

Haiden, T., A. Kann, C. Wittmann, G. Pistotnik, B. Bica, and C. Gruber, 2011: The Integrated Nowcasting through Comprehensive Analysis (INCA) system and its validation over the eastern alpine region. *Wea. Forecasting*, **26**, 166–183, https://doi.org/10.1175/2010WAF2222451.1.

Hofstätter, M., A. Lexer, M. Homann, and G. Blöschl, 2018: Large-scale heavy precipitation over central Europe and the role of atmospheric cyclone track types. *Int. J. Climatol.*, **38**, e497–e517, https://doi.org/10.1002/joc.5386.

Huff, F. A., 1995: Characteristics and contributing causes of an abnormal frequency of flood-producing rainstorms at Chicago. *J. Amer. Water Resour. Assoc.*, **31**, 703–714, https://doi.org/10.1111/j.1752-1688.1995.tb03395.x.

——, and W. L. Shipp, 1969: Spatial correlations of storm, monthly and seasonal precipitation. *J. Appl. Meteor.*, **8**, 542–550, https://doi.org/10.1175/1520-0450(1969)008<0542:SCOSMA>2.0.CO;2.

Kang, B., E. Kim, J. G. Kim, and S. Moon, 2019: Comparative study on spatiotemporal characteristics of fixed-area and storm-centered ARFs. *J. Hydrol. Eng.*, **24**, 04019044, https://doi.org/10.1061/(ASCE)HE.1943-5584.0001839.

Koutsoyiannis, D., 2004a: Statistics of extremes and estimation of extreme rainfall: II. Empirical investigation of long rainfall records. *Hydrol. Sci. J.*, **49**, 591–610, https://doi.org/10.1623/hysj.49.4.591.54424.

——, 2004b: Statistics of extremes and estimation of extreme rainfall: I. Theoretical investigation. *Hydrol. Sci. J.*, **49**, 575–590, https://doi.org/10.1623/hysj.49.4.575.54430.

——, and G. Baloutsos, 2000: Analysis of a long record of annual maximum rainfall in Athens, Greece, and design rainfall inferences. *Nat. Hazards*, **22**, 29–48, https://doi.org/10.1023/A:1008001312219.

Le, P. D., A. C. Davison, S. Engelke, M. Leonard, and S. Westra, 2018: Dependence properties of spatial rainfall extremes and areal reduction factors. *J. Hydrol.*, **565**, 711–719, https://doi.org/10.1016/j.jhydrol.2018.08.061.

Lombardo, F., F. Napolitano, and F. Russo, 2006: On the use of radar reflectivity for estimation of the areal reduction factor. *Nat. Hazard Earth Syst.*, **6**, 377–386, https://doi.org/10.5194/nhess-6-377-2006.

Mailhot, A., I. Beauregard, G. Talbot, D. Caya, and S. Biner, 2012: Future changes in intense precipitation over Canada assessed from multi-model NARCCAP ensemble simulations. *Int. J. Climatol.*, **32**, 1151–1163, https://doi.org/10.1002/joc.2343.

Mair, A., and A. Fares, 2011: Comparison of rainfall interpolation methods in a mountainous region of a tropical island. *J. Hydrol. Eng.*, **16**, 371–383, https://doi.org/10.1061/(ASCE)HE.1943-5584.0000330.

Marston, F. A., 1924: The distribution of intense rainfall and some other factors in the design of storm-water drains. *Proc. Amer. Soc. Civ. Eng.*, **50**, 19–46.

Merz, R., and G. Blöschl, 2003: A process typology of regional floods. *Water Resour. Res.*, **39**, 1340, https://doi.org/10.1029/2002WR001952.

Mineo, C., E. Ridolfi, F. Napolitano, and F. Russo, 2018: The areal reduction factor: A new analytical expression for the lazio region in central Italy. *J. Hydrol.*, **560**, 471–479, https://doi.org/10.1016/j.jhydrol.2018.03.033.

Müller, H., and U. Haberlandt, 2018: Temporal rainfall disaggregation using a multiplicative cascade model for spatial application in urban hydrology. *J. Hydrol.*, **556**, 847–864, https://doi.org/10.1016/j.jhydrol.2016.01.031.

Myers, V. A., and R. M. Zehr, 1980: A methodology for point-to-area rainfall frequency ratios. NOAA Tech. Rep. NWS 24, 176 pp., http://www.nws.noaa.gov/oh/hdsc/Technical_reports/TR24.pdf.

NERC, 1975: *Flood Studies Report*. Vol. II, Natural Environment Research Council, 81 pp.

Okoli, K., K. Breinl, L. Brandimarte, A. Botto, E. Volpi, and G. Di Baldassarre, 2018: Model averaging versus model selection: Estimating design floods with uncertain river flow data. *Hydrol. Sci. J.*, **63**, 1913–1926, https://doi.org/10.1080/02626667.2018.1546389.

Olivera, F., J. Choi, D. Kim, and M. H. Li, 2008: Estimation of average rainfall areal reduction factors in Texas using NEXRAD data. *J. Hydrol. Eng.*, **13**, 438–448, https://doi.org/10.1061/(ASCE)1084-0699(2008)13:6(438).

Omolayo, A. S., 1993: On the transposition of areal reduction factors for rainfall frequency estimation. *J. Hydrol.*, **145**, 191–205, https://doi.org/10.1016/0022-1694(93)90227-Z.

Pebesma, E. J., and C. G. Wesseling, 1998: Gstat: A program for geostatistical modelling, prediction and simulation. *Comput. Geosci.*, **24**, 17–31, https://doi.org/10.1016/S0098-3004(97)00082-4.

Peel, M. C., B. L. Finlayson, and T. A. McMahon, 2007: Updated world map of the Koppen-Geiger climate classification. *Hydrol. Earth Syst. Sci.*, **11**, 1633–1644, https://doi.org/10.5194/hess-11-1633-2007.

Poduje, A. C. C., and U. Haberlandt, 2018: Spatio-temporal synthesis of continuous precipitation series using vine copulas. *Water*, **10**, 862, https://doi.org/10.3390/w10070862.

Ramos, M. H., J. D. Creutin, and E. Leblois, 2005: Visualization of storm severity. *J. Hydrol.*, **315**, 295–307, https://doi.org/10.1016/j.jhydrol.2005.04.007.

Rodriguez-Iturbe, I., and J. M. Mejía, 1974: On the transformation of point rainfall to areal rainfall. *Water Resour. Res.*, **10**, 729–735, https://doi.org/10.1029/WR010i004p00729.

Schulz, W., K. Cummins, G. Diendorfer, and M. Dorninger, 2005: Cloud-to-ground lightning in Austria: A 10-year study using data from a lightning location system. *J. Geophys. Res.*, **110**, D09101, https://doi.org/10.1029/2004JD005332.

Seibert, P., A. Frank, and H. Formayer, 2007: Synoptic and regional patterns of heavy precipitation in Austria. *Theor. Appl. Climatol.*, **87**, 139–153, https://doi.org/10.1007/s00704-006-0198-8.

Sivapalan, M., and G. Blöschl, 1998: Transformation of point rainfall to areal rainfall: Intensity-duration frequency curves. *J. Hydrol.*, **204**, 150–167, https://doi.org/10.1016/S0022-1694(97)00117-0.

Skaugen, T., 1997: Classification of rainfall into small- and large-scale events by statistical pattern recognition. *J. Hydrol.*, **200**, 40–57, https://doi.org/10.1016/S0022-1694(97)00003-6.

Skøien, J. O., and G. Blöschl, 2006: Catchments as space-time filters – A joint spatio-temporal geostatistical analysis of runoff and precipitation. *Hydrol. Earth Syst. Sci.*, **10**, 645–662, https://doi.org/10.5194/hess-10-645-2006.

Svensson, C., and D. A. Jones, 2010: Review of methods for deriving areal reduction factors. *J. Flood Risk Manag.*, **3**, 232–245, https://doi.org/10.1111/j.1753-318X.2010.01075.x.

U.S. Weather Bureau, 1957: Rainfall intensity-frequency regime: Part 1—The Ohio Valley. Weather Bureau Tech. Paper 29, 44 pp., https://www.nws.noaa.gov/oh/hdsc/Technical_papers/TP29P1.pdf.

——, 1958: Rainfall intensity-frequency regime: Part 2—Southeastern United States. Weather Bureau Tech. Paper 29, 51 pp., https://www.nws.noaa.gov/oh/hdsc/Technical_papers/TP29P2.pdf.

Veneziano, D., and A. Langousis, 2005: The areal reduction factor: A multifractal analysis. *Water Resour. Res.*, **41**, W07008, https://doi.org/10.1029/2004WR003765.

Verworn, H. R., 2008: Flächenabhängige abminderung statistischer regenwerte. *Korresp. Wasserwirtsch.*, **1**, 493–498.

Wagner, P. D., P. Fiener, F. Wilken, S. Kumar, and K. Schneider, 2012: Comparison and evaluation of spatial interpolation schemes for daily rainfall in data scarce regions. *J. Hydrol.*, **464–465**, 388–400, https://doi.org/10.1016/j.jhydrol.2012.07.026.

Walsh, K. M., M. A. Cooper, R. Holle, V. A. Rakov, W. P. Roeder, and M. Ryan, 2013: National athletic trainers' association position statement: Lightning safety for athletics and recreation. *J. Athletic Train.*, **48**, 258–270, https://doi.org/10.4085/1062-6050-48.2.25.

Wright, D. B., J. A. Smith, and M. L. Baeck, 2014: Critical examination of area reduction factors. *J. Hydrol. Eng.*, **19**, 769–776, https://doi.org/10.1061/(ASCE)HE.1943-5584.0000855.

Zehr, R. M., and V. A. Myers, 1984: Depth-area ratios in the semi-arid southwest United States. NOAA Tech. Memo. NWS HYDRO-40, 45 pp., https://www.nws.noaa.gov/oh/hdsc/Technical_memoranda/TM40.pdf.